Scientific Research Publishing

Open Journal of Fluid Dynamics, 2025, 15(2), 47-63
https://www.scirp.org/journal/ojfd
ISSN Online: 2165-3860
ISSN Print: 2165-3852

Analysis of the Effect of Temperature on MHD Electrical Power Generation with Lattice Boltzmann Method

Daniel Azure Ayine[1*], Rabiu Musah[2], Christian John Etwire[3]

[1]Department of Mathematics, School of Mathematical Sciences, C. K. Tedam University of Technology and Applied Sciences, Navrongo, Ghana
[2]Department of Physics, Faculty of Physical Sciences, University for Development Studies, Nyankpala Campus, Tamale, Ghana
[3]Department of Mathematics, School of Mathematical Sciences, C. K. Tedam University of Technology and Applied Sciences, Navrongo, Ghana
Email: *dayine.stu@cktutas.edu.gh, mrabiu@uds.edu.gh, cetwire@cktutas.edu.gh

How to cite this paper: Ayine, D.A., Musah, R. and Etwire, C.J. (2025) Analysis of the Effect of Temperature on MHD Electrical Power Generation with Lattice Boltzmann Method. *Open Journal of Fluid Dynamics*, **15**, 47-63.
https://doi.org/10.4236/ojfd.2025.152004

Received: February 4, 2025
Accepted: April 22, 2025
Published: April 25, 2025

Abstract

The flow of electrically conducting fluids is vital in engineering applications such as Magneto-hydro-dynamic (MHD) generators, Fusion reactors, cooling systems, and Geo-physics. In this study, a mathematical model has been formulated to investigate the effect of temperature on power generation in different sections of an MHD Generator with salt solution (Seawater) as the working fluid. Also, the Lattice Boltzmann method was employed to simulate the fluid flow in an MHD generator for different inlet temperatures in Python. The impact of the working fluid's inlet temperature on power generation has been established by varying the inlet temperature of the working fluid. The temperature, velocity, and electrical power profiles along and across the generator channel have been extracted and analyzed. The results affirm and complement the findings of experimental and analytical studies of MHD power generation. The study established that high temperature enhances velocity and pressures at the inlet, facilitating ionization and conductivity of the working fluid and resulting in peak electric power within one-fifth of the generator channel. Reduction in temperature towards the outlet results in decreased ionization and low conductivity of the working fluid, accounting for a decline in electric power. The study further revealed that maximum power is obtained from the inlet region along a three-fifths section of the generator. The power then declines in the last two-fifths of the generator channel and stabilizes asymptotically towards the outlet.

Keywords

Electrically Conducting Fluid, Lattice Boltzmann Method, Electrodes, Velocity Set, Power Generator, Working Fluid

1. Introduction

A magneto-hydro-dynamics (MHD) power generator is a device that generates electric power using the interaction of moving electrically conducting fluid and a magnetic field, Sivasubramanian [1]. Electrically conducting fluids are ionized gases (plasma) and liquid metals such as mercury or sodium, Krishan [2]. The presence of ions and free electrons in an electrically conducting fluid makes it suitable as a working fluid in an MHD power generator.

The advantages of the MHD generator are that it consumes less fuel and produces pollution-free power. It can reach full power level as soon as it is started and is usually smaller than conventional fossil fuel plants, Awais *et al.* [3]. Also, Bera [4] stated that MHD power generation is very promising in multimodal power generation systems when coupled with the thermal power plant. With the development of computational fluid dynamics and other computer simulation tools, opportunities to explore the MHD technique and the systems are open in recent times. More research investigations are required in various parts of the MHD systems, such as fluid, electrodes, magnetic field, and the system geometry.

Most of the research in MHD power generation is experimental studies in which the working fluid is ionized inert gases such as Argon, Xenon, and Neon, together with seed elements to enhance the conductivity of the gas. The seed elements used are ionizable materials such as Potassium, Cesium, and other alkaline compounds, which are dangerous when discharged into the environment. Yiwen *et al.* [5] presented a preliminary experimental investigation on MHD power generation using seeded supersonic argon flow as a working fluid. The segmented MHD power generator's induction voltage and short-circuit current were measured. They observed a decline in performance caused by electrode oxidation and low magnetic field strength created by permanent magnets.

According to Jinshah *et al.* [6], the low conductivity property of gas at high temperatures is the main source of issues in MHD power generation. They indicated that the thermal energy of the gas is directly turned into electrical energy when a high-temperature, high-velocity conductor is passed through a strong magnetic field. However, Sene *et al.* [7] reported that thermal effects were insignificant after they carried out their experiment at room temperature without using any cooling or heating equipment. Rosa *et al.* [8] discovered that there are essentially no maximum limitations to the temperature that an MHD generator can tolerate after studying Plasma flow in an MHD Power Generation system. They observed that the Hall effect accentuates an unevenness of the temperature. Therefore, the electrical conductivity of the plasma decreased as the wall was approached, which caused a voltage drop across the thermal boundary layer.

Tanaka *et al.* [9] in their experiment analyzed the impact of temperature on the efficiency and stability of the generator. It was observed that the power output increased monotonically with temperature, but the enthalpy extraction ratio saturated at high inlet total temperatures exceeding 8000 K. They found that between 6500 K and 7000 K, the plasma transitioned from a homogenous and stable state; however, the stable plasma properties and structure are not significantly impacted by load resistance.

Wang *et al.* [10] analyzed the performance of a Liquid Metal MHD enhanced Closed Brayton Cycle (CBC) system coupled with a scramjet, revealing significant insights into power generation capabilities. A multi-stage hybrid-separation LMMHD generator was proposed, which effectively decouples the void fraction of the MHD channel from the wall cooling process, allowing for better control of the void fraction by adjusting the number of stages. Their results indicated that increasing the void fraction benefits overall power generation performance. Ork *et al.* [11] experimented in a shock-tube facility to test Magnetohydrodynamic electrical power generation. They obtained an enthalpy extraction ratio of about 5.0% by using a disk-shaped MHD generator with radio frequency pre-ionization.

Kimsor *et al.* [12] demonstrated that pre-ionized inert gas plasma can effectively generate electrical power through MHD processes, achieving an enthalpy extraction ratio of 4.01% in a disk-shaped generator with radio-frequency pre-ionization.

Domínguez-Lozoya [13], in their review of MHD power generation for sustainable development, proposed converting ocean energy, specifically waves and tides, into electricity using MHD generators that utilize seawater or liquid metal as working fluids. Aoki *et al.* [14] examined the effect of a magnetic field on seawater electrolysis by conducting a simulation in a linear-type seawater magnetohydrodynamic power generator. They detailed the construction of experimental equipment and an electrochemical flow cell designed for the linear-type seawater magnetohydrodynamic (MHD) power generator. Their effort is crucial for studying the effects of magnetic fields on seawater electrolysis and MHD power generation.

According to Takeda *et al.* [15], a seawater MHD power generator is a unique system that directly transforms seawater flow's kinetic energy into electric energy and generates hydrogen gas as a by-product. In their experiment, the electromotive force and the generator output were small under the influence of a large flow loss of the generator.

The literature indicates that most research on MHD power generation is experimental, utilizing gas as the working fluid. However, few studies explore the prospect of using salt solution (seawater) as the working fluid in MHD generators, hence the need for further research.

1.1. Novelty

Since most studies on MHD electrical power generation are either experimental or analytical, the current research mathematically models and simulates the flow

of hot salt solution (seawater) as a working fluid to help improve understanding of power generation in different sections of the MHD generator using the Lattice Boltzmann method (LBM).

1.2. Applications

The findings of this study will help provide knowledge to enhance the production of clean, renewable, and cheap MHD electric power for domestic and industrial use. It would also help protect the environment since MHD generators that use seawater as a working fluid do not necessarily need seeding elements to make it conductive, as required in gaseous working fluids.

2. Description of the Problem

An incompressible electrically conducting fluid such as salt solution (seawater) is assumed to flow through an MHD generator duct, where the top and bottom plates are electrodes and the side plates are insulating walls. A magnetic field is imposed perpendicularly on the insulated surfaces. A Cartesian coordinate system is adopted for this study so that the working fluid flows along the x-direction through the channel. Electrodes are placed inclined to the channel to form a wedge-like shape. A magnetic field is then imposed along the z-direction. A heated salt solution with an even temperature of 0.5 lattice units (423.15 K) is injected into the channel of the MHD Generator. The temperature of the working fluid is later increased to study the effect of temperature on power generation. The geometric model of the MHD generator is shown below in Figure 1.

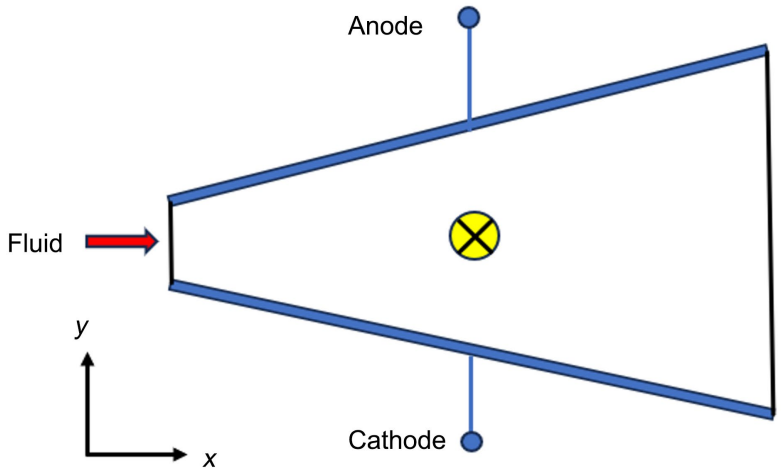

Figure 1. MHD power generator.

2.1. Mathematical Model of the Problem

The fluid flow geometry described above is mathematically modeled by the following governing equations: Continuity, Momentum, and Magnetic induction, from Equations (1) to (3) as in Foldes *et al.* [16] and Equation (4) which is the energy equation.

$$\frac{\partial \rho}{\partial t}+\frac{\partial u}{\partial x}+\frac{\partial v}{\partial y}=0. \tag{1}$$

$$\frac{\partial u}{\partial t}+u\frac{\partial u}{\partial x}+v\frac{\partial u}{\partial y}=-\frac{\partial P}{\partial x}+\nu\frac{\partial^2 u}{\partial y^2}+s_u. \tag{2}$$

$$\frac{\partial B}{\partial t}+u\frac{\partial B}{\partial x}+v\frac{\partial B}{\partial y}=\eta\frac{\partial^2 B_y}{\partial y^2}. \tag{3}$$

$$\frac{\partial T}{\partial t}+u\frac{\partial T}{\partial x}+v\frac{\partial T}{\partial y}=\alpha_0\frac{\partial^2 T}{\partial y^2}+s_t. \tag{4}$$

The above system of equations models the non-steady incompressible fluid flow in the MHD generator. In the system of equations, ρ is density and u and v are velocities in the x and y directions respectively. Also, B and T are magnetic and temperature fields respectively. In addition, ν, σ and α_0 represent kinematic viscosity, electrical conductivity, and thermal diffusion coefficient respectively. Also, S_u and S_t in Equations (2) and (4) are the momentum and energy source terms respectively. The effect of the imposed magnetic field on the fluid is modeled with the magnetic induction Equation (3) obtained from Ohm's law and Maxwell's equations. In this study $S_t=0$, however, the momentum source term S_u is denoted by the Boussinesq approximation such that,

$$S_u=g\beta_T\left(T-T_0\right). \tag{5}$$

Equation (5) models the Buoyancy force due to thermal diffusion where β_T is the coefficient of thermal expansion, g is the acceleration due to gravity, T is the temperature of the system and T_0 is the initial temperature of the working fluid.

2.2. Boundary Conditions

At the starting point of the flow through the MHD generator, the variables dictating the flow assume the following values,

$$\begin{cases} t=0: u\left(x,0\right)=U_0, v\left(x,0\right)=0, \\ B\left(x,0\right)=0, T\left(x,0\right)=T_0. \end{cases} \tag{6}$$

The boundary conditions of the system at the lower and upper walls (electrodes), where L is the length of the channel and h is the distance between the two electrodes, are stated below,

$$\begin{aligned} &0<x<L: u\left(x,y\right)=0, B\left(x,y\right)=0, T\left(x,y\right)=T_w, \text{ at } y=0, \\ &0<x<L: u\left(x,y\right)=0, B\left(x,y\right)=0, T\left(x,y\right)=T_w, \text{ at } y=h. \end{aligned} \tag{7}$$

In Equations (7), T_w is the temperature at the plate surface. The fluid flow variables across the MHD channel assume the following initial values,

$$t>0: u=U_o, v=0, T=T_0, B=B_0 \text{ at } y=\pm h. \tag{8}$$

From Equations (6) to (8), U_0, T_0, and B_0 denote initial velocity, temperature, and magnetic field respectively.

The Lattice Boltzmann method is then adopted to simulate the fluid flow in the MHD generator channel.

3. Problem Formulated with Lattice Boltzmann Method

The Boltzmann transport equation in kinetic theory is obtained from the total derivative of the particle distribution function, $f(\boldsymbol{x},\boldsymbol{\xi},t)$ where $\boldsymbol{x}$ is a spatial variable, $\boldsymbol{\xi}$ is velocity and, t denotes time. The total derivative of the distribution function is shown below,

$$\frac{\mathrm{d}f}{\mathrm{d}t}=\frac{\partial f}{\partial t}+\boldsymbol{\xi}\frac{\partial f}{\partial \boldsymbol{x}}+\frac{F}{m}\frac{\partial f}{\partial \boldsymbol{\xi}}=\Omega(f), \tag{9}$$

where F is force, m is mass and $\Omega(f)$ is the collision operator. The collision operator is simplified by using the Bhatnagar-Gross-Krook (BGK) collision operator shown in Equation (10) as in Mora *et al.* [17],

$$\Omega(f)=-\left(\frac{f_i-f^{eq}}{\tau}\right), \tag{10}$$

where f^{eq} is the equilibrium distribution function. The equilibrium distribution function f^{eq} is defined by the Boltzmann distribution function as:

$$f^{eq}(\rho,u)=\frac{\rho}{(2\pi RT)^{D/2}}\exp\left(-\frac{(c-\boldsymbol{u})^2}{2RT}\right), \tag{11}$$

where D denotes the number of dimensions, R is the specific gas constant, T is temperature and c_s is the speed of sound such that $c_s=\sqrt{RT}$ and lattice speed $c=\dfrac{\Delta x}{\Delta t}$.

The equilibrium distribution function in Equation (11) is simplified by using Taylor series expansion to obtain,

$$f^{eq}(\rho,u)=w_\alpha\rho\left(1+\frac{\boldsymbol{u}\cdot c_\alpha}{c_s^2}+\frac{(\boldsymbol{u}c_\alpha)^2}{2c_s^4}-\frac{\boldsymbol{u}\cdot\boldsymbol{u}}{2c_s^2}\right), \tag{12}$$

where ρ is macroscopic density, $\boldsymbol{u}$ is macroscopic velocity, w_α is the weight of the velocity set of the distribution of the particles, c_α is discrete velocities and c_s is the speed of sound. Also, the speed of sound $c_s^2=\dfrac{1}{3}\left(\dfrac{\Delta x}{\Delta t}\right)^2$. The Macroscopic density is defined as,

$$\rho=\sum_{\alpha=0}^{8}f_\alpha. \tag{13}$$

The macroscopic velocity is obtained from the momentum of the distribution defined as,

$$\rho u=\sum_{\alpha=0}^{8}f_\alpha\cdot\boldsymbol{c}_\alpha. \tag{14}$$

In this study, we adopt the D_2Q_9 Velocity set as in Mohamad [18] shown below in **Figure 2**, since the study is a two-dimensional fluid flow analysis between the MHD generator's lower and upper walls (electrodes).

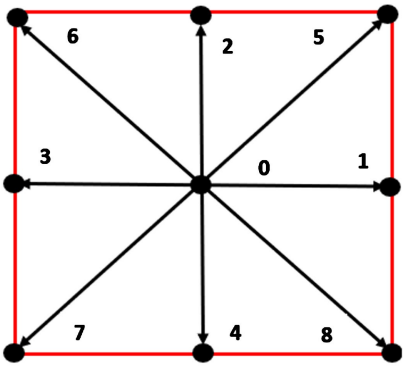

Figure 2. D_2Q_9 velocity set.

The velocities c_α in the various directions α for D_2Q_9 are stated below,

$$\begin{cases} \boldsymbol{c}_0 = (0,0), \boldsymbol{c}_1 = (1,0), \boldsymbol{c}_2 = (0,1), \\ \boldsymbol{c}_3 = (-1,0), \boldsymbol{c}_4 = (0,-1), \boldsymbol{c}_5 = (1,1), \\ \boldsymbol{c}_6 = (-1,1), \boldsymbol{c}_7 = (-1,-1), \boldsymbol{c}_8 = (1,-1). \end{cases} \tag{15}$$

At the wall boundaries, the fluid particles bounce back into the fluid, and the velocities of such particles are represented by opposite directions called "no slip" directions,

$$\text{no slip} = [0,3,4,1,2,7,8,5,6]. \tag{16}$$

Also, the weights associated with the various velocity directions for the D_2Q_9 as in Mohamad [18] are,

$$\begin{cases} w_0 = \dfrac{4}{9}, \quad w_1 = w_2 = w_3 = w_4 = \dfrac{1}{9}, \\ w_5 = w_6 = w_7 = w_8 = \dfrac{1}{36}. \end{cases} \tag{17}$$

3.1. Momentum Equation Using Lattice Boltzmann Method

To model the momentum of the fluid flow, we discretize Equation (9). Let $\xi \equiv \boldsymbol{c}_\alpha$ where $\boldsymbol{c}_\alpha$ denote a discrete velocity set. Then the discretized Lattice Boltzmann momentum equation with the BGK collision operator without the force terms in Xiong [19] is shown as Equation (18) below,

$$f_\alpha(\boldsymbol{x} + \boldsymbol{c}_\alpha \Delta t, t + \Delta t) - f_\alpha(\boldsymbol{x}, t) = -\left(\frac{f_\alpha - f_\alpha^{eq}}{\tau}\right). \tag{18}$$

The macroscopic parameters, such as the working fluid's density and velocity, are obtained from the distribution function, as in Equations (13) and (14), respectively.

3.2. Magnetic Induction Equation with Lattice Boltzmann Method

The Magnetic induction equation is represented in LBM as follows. We let $z_\alpha(\boldsymbol{x}_\alpha, t)$ be the magnetic distribution function, then the magnetic induction equation is written in LBM form as,

$$z_\alpha\left(\boldsymbol{x}+\boldsymbol{c}_\alpha\Delta t,t+\Delta t\right)-z_\alpha\left(\boldsymbol{x},t\right)=\frac{1}{\tau_m}\left(z_\alpha\left(\boldsymbol{x},t\right)-z_\alpha^{eq}\left(\boldsymbol{x},t\right)\right), \tag{19}$$

where τ_m is the magnetic relaxation time, z_α^{eq} is the magnetic equilibrium distribution function. The magnetic field density of the system is obtained as,

$$B=\sum_{\alpha=0}^{8} z_\alpha. \tag{20}$$

The equilibrium distribution function of the magnetic field z_α^{eq} is given in Jamali *et al.* [20] as,

$$z_\alpha^{eq}=w_\alpha\left(\boldsymbol{B}_\beta+3c_\alpha\left(u_\alpha B_\beta-B_\alpha u_\beta\right)\right), \tag{21}$$

where w_α are the lattice weights for the magnetic field.

The LBM for the momentum source term in Miyan [21] is modeled as,

$$S_u=3w_\alpha g_x\beta_T\theta c_x+3w_\alpha g_y\beta_T\theta c_y. \tag{22}$$

where w_α denote lattice weights, g_x and g_y are gravity components, β_T is the thermal Buoyancy coefficient. Also, θ is the temperature of the system and c_x, c_y are lattice directions.

3.3. Energy Equation with Lattice Boltzmann Method

The energy distribution function $h_\alpha\left(\boldsymbol{x},t\right)$ is defined as,

$$h_\alpha\left(\boldsymbol{x}+\boldsymbol{c}_\alpha\Delta t,t+\Delta t\right)-h_\alpha\left(\boldsymbol{x},t\right)=-\frac{1}{T_T}\left(h_\alpha\left(\boldsymbol{x},t\right)-h_\alpha^{eq}\left(\boldsymbol{x},t\right)\right), \tag{23}$$

where T_T is the thermal relaxation time and h_α^{eq} is the thermal equilibrium distribution function. The thermal equilibrium distribution function of the energy equation h_α^{eq} is given in Krüger *et al.* [22] as,

$$h_\alpha^{eq}=w_\alpha T\left(1+\frac{\boldsymbol{u}\cdot c_\alpha}{c_s^2}+\frac{\left(\boldsymbol{u}c_\alpha\right)^2}{2c_s^4}-\frac{\boldsymbol{u}\cdot\boldsymbol{u}}{2c_s^2}\right), \tag{24}$$

where W_α is the weight of the thermal distribution direction (α) and the temperature T of the system is estimated as,

$$T=\sum_{\alpha=0}^{8} h_\alpha. \tag{25}$$

3.4. Boundary Conditions

We employ a periodic boundary technique at the inlet and outlet of the MHD power generator system and a bounce-back boundary technique at the system's electrodes (wall). Assuming periodicity along the x direction, the inlet and outlet boundary conditions for the momentum equation are as in Equation (26) and Equation (27) respectively:

$$f\left(0,:,i\right)=f^{eq}\left(0,:,i\right)+f\left(0,:,noslip\left(i\right)\right)-f^{eq}\left(0,:,noslip\left(i\right)\right) \quad \text{for } i=1,5,8, \tag{26}$$

and,

$$f\left(-1,:,i\right)=f\left(-2,:,i\right) \quad \text{for } i=3,6,7. \tag{27}$$

The bottom and top momentum boundary conditions at the electrodes of the generator are,

$$f\left(bot_{block},i\right)=Vinlet*\left(wFluid\left[i\right]+wFluid\left[noslip\left[i\right]\right]\right)-f\left[bot\_block,noslip\left[i\right]\right]\quad \text{for } i=2,5,6, \tag{28}$$

$$f\left[top\_block,i\right]=Vinlet*\left(wFluid\left[i\right]+wFluid\left[noslip\left[i\right]\right]\right)-f\left[top\_block,noslip\left[i\right]\right]\quad \text{for } i=4,7,8. \tag{29}$$

The magnetic boundary conditions are as shown below,

$$z_y\left[0,:,i\right]=-z_y\left[0,:,noslip\left[i\right]\right]\quad \text{for } i=1,5,8, \tag{30}$$

$$z_x\left[0,:,i\right]=-z_x\left[0,:,noslip\left[i\right]\right]\quad \text{for } i=1,5,8, \tag{31}$$

$$z_x\left[-1,:,i\right]=-z_x\left[-1,:,noslip\left[i\right]\right]\quad \text{for } i=3,6,7, \tag{32}$$

$$z_y\left[-1,:,i\right]=-z_y\left[-1,:,noslip\left[i\right]\right]\quad \text{for } i=3,6,7. \tag{33}$$

The thermal energy inlet and outlet boundary conditions are as in Equations (34) and (35),

$$h\left[0,:,i\right]=Tinlet*\left(wTemp\left[i\right]+wTemp\left[noslip\left[i\right]\right]\right)-h\left[0,:,noslip\left[i\right]\right]\quad \text{for } i=1,5,8, \tag{34}$$

$$h\left[-1,:,i\right]=h\left[-2,:,i\right]\quad \text{for } i=3,6,7. \tag{35}$$

The bottom and top thermal boundary conditions are as in Equation (36) and (37),

$$h\left[bot\_block,i\right]=Tinlet*\left(wTemp\left[i\right]+wTemp\left[noslip\left[i\right]\right]\right)-h\left[bot\_block,noslip\left[i\right]\right]\quad \text{for } i=2,5,6, \tag{36}$$

$$h\left[top\_block,i\right]=Tinlet*\left(wTemp\left[i\right]+wTemp\left[noslip\left[i\right]\right]\right)-h\left[top\_block,noslip\left[i\right]\right]\quad \text{for } i=4,7,8. \tag{37}$$

Table 1 contains dimensionless parameters of the MHD generator, physical properties of the working fluid (salt solution/seawater) and other parameters associated with the Lattice Boltzmann Method in lattice units used for the simulation. Equations (18), (19), and (23) are simulated in Python with the specified boundary conditions from Equations (26) to (37) and the dimensionless parameter values presented in Table 1.

Table 1. Dimensionless simulation parameter values.

Parameter	Symbol	Values in Lattice Units
Initial Velocity	u_0	0.4
Inlet Temperature of fluid	θ_i	0.5
Initial Magnetic field	B_0	1.0

Continued

Density of fluid	ρ_0	1.0
Temperature of wall (Electrodes)	θ_w	0.1
Thermal Expansion coefficient	β_T	0.00001
Renolds Number	Re	200
Prandtl Number	Pr	0.6
Dynamic Viscosity	μ	0.126
Electrical Conductivity of Fluid	σ	4.31
Electrode Conductivity	σ_e	1.5
Length of Generator	l	2^8
Width of Generator	w	2^6
Fluid Collision Time	ω_f	0.001
Thermal Collision Time	ω_T	0.012
Magnetic Collision Time	ω_m	0.011
Magnetic Renolds Number	Re_m	0.9
Magnetic Prandtl Number	Pr_m	0.6

4. Results and Discussions

The orientations of the walls (electrodes) of the MHD generator in this study are inclined to form a wedged-like shape, as shown in Figure 1. However, to validate the results of this study, the orientations of the electrodes were set parallel to each other to obtain the standard geometry for Poiseuille flow and the numerical solution of the cross-sectional velocity profile of the channel compared with the analytic solution of the Poiseuille velocity profile, Wu *et al.* [23] as shown in Equation (38),

$$u = -\frac{h^2}{2\mu}\frac{\mathrm{d}p}{\mathrm{d}x}\left(1-\left(\frac{y}{h}\right)^2\right). \tag{38}$$

Figure 3 shows the relationship between the present numerical result using the dimensionless parameters in Table 1, compared to the analytical result of Equation (38). The simulation was implemented in Python by setting some of the parameters in Table 1 to zero, *i.e.*, $\theta_i = \theta_e = \beta_T = B_0 = Re_m = \sigma = \sigma_e = 0$ and the result compared with the benchmark Poiseuille flow profile.

4.1. Velocity Profile in the MHD Generator

The velocity profile across different sections of the MHD generator channel is shown below in Figure 4.

Figure 4 shows that the velocity across the channel at one-fifth of the channel length is fully developed and high; however, it reduces at four-fifths of the channel towards the outlet. The reduction in velocity of the working fluid is due to viscous forces at the walls, Lorentz force in the bulk of the working fluid, and the large width of the outlet.

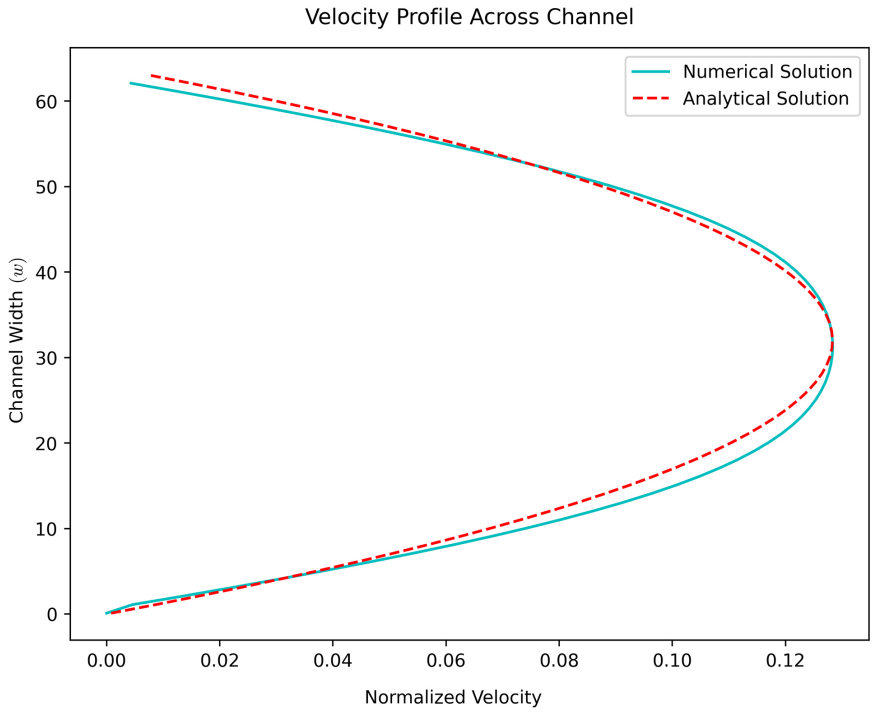

Figure 3. Poiseuille velocity profile.

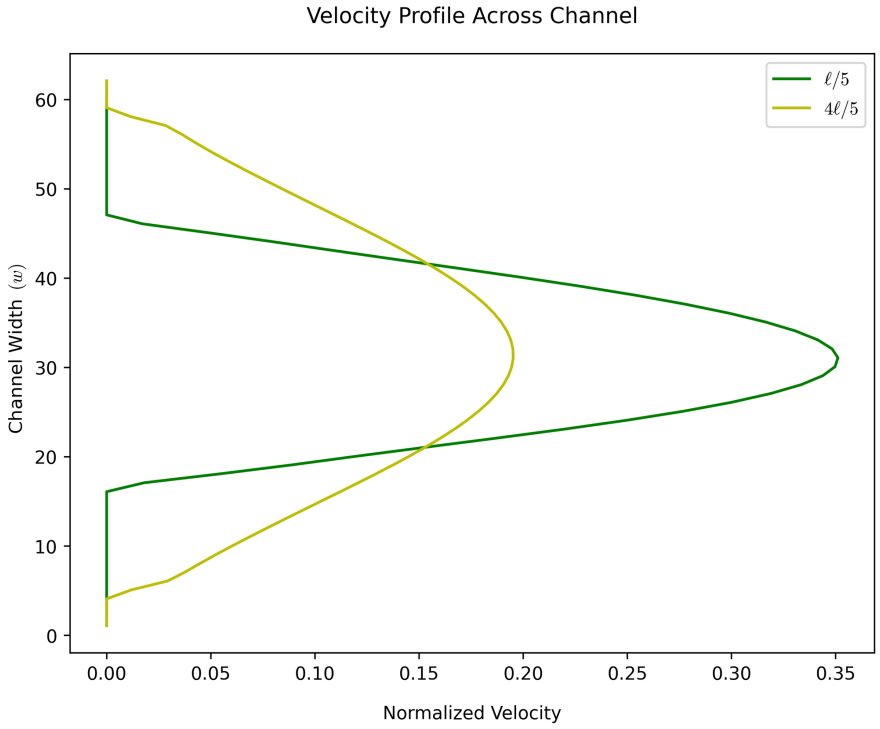

Figure 4. Velocity profile across the MHD generator channel.

4.2. Temperature Profile in MHD Generator

The temperature profile of the working fluid in the MHD generator is shown below in **Figure 5**.

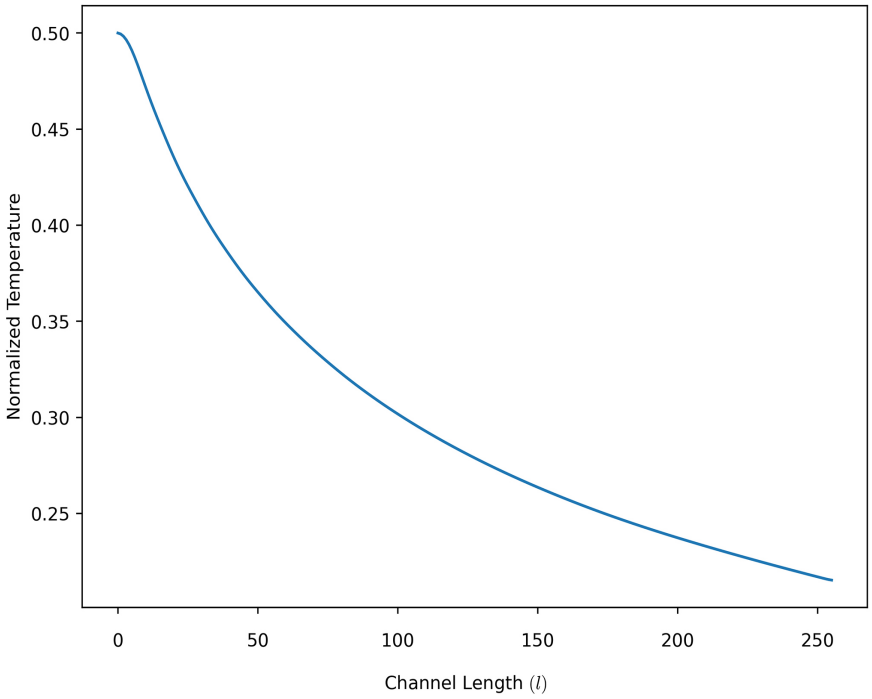

Figure 5. Temperature profile of working fluid in the MHD generator.

As can be observed in **Figure 5**, the working fluid's temperature declines gradually along the channel towards the exit. An initial inlet temperature of 0.5 lattice units gradually dropped to about 0.2 lattice units towards the outlet of the MHD generator channel, which denotes a 60% drop in inlet temperature. The reduced temperature of the working fluid was due to heat loss at the electrodes/walls.

4.3. Electric Power Profile in the MHD Generator

The electric power, $\overline{P}$ per unit length from the MHD generator is obtained by using Equation (39) as presented by Miyan [21] and E-sparX [24] given as,

$$\overline{P} = \frac{\sigma u B^2}{\rho} \tag{39}$$

where σ is the electrical conductivity of the working fluid, u is the velocity, B is the magnetic flux density of the system and ρ is the density of the working fluid. In this study, the net magnet flux B is the difference between the imposed magnetic flux B_0 and the induced magnetic flux due to Lorentz force, $B_{ind} = \sqrt{b_x^2 + b_y^2}$. Therefore, the power $\overline{P}$ in this study is computed by using Equation (40),

$$\overline{P} = \frac{\sigma u \left(B_0 - B_{ind} \right)^2}{\rho}. \tag{40}$$

Figures 6-8 show the electrical power profiles in the MHD generator as color-mapped images and line graphs extracted along and across the generator's channel.

At a constant wall (electrode) temperature of 0.1 lattice units, the various Figures represent the power produced at three different inlet temperatures of the working fluid (salt solution). In Figure 6, when the inlet temperature was 0.5, the electric power produced in the generator increased from 0.4 to peak at 0.7 in the first one-fifth of the channel. It then gradually dropped and stabilized to 0.2 towards the exit, as in Figure 6(b) and Figure 6(c).

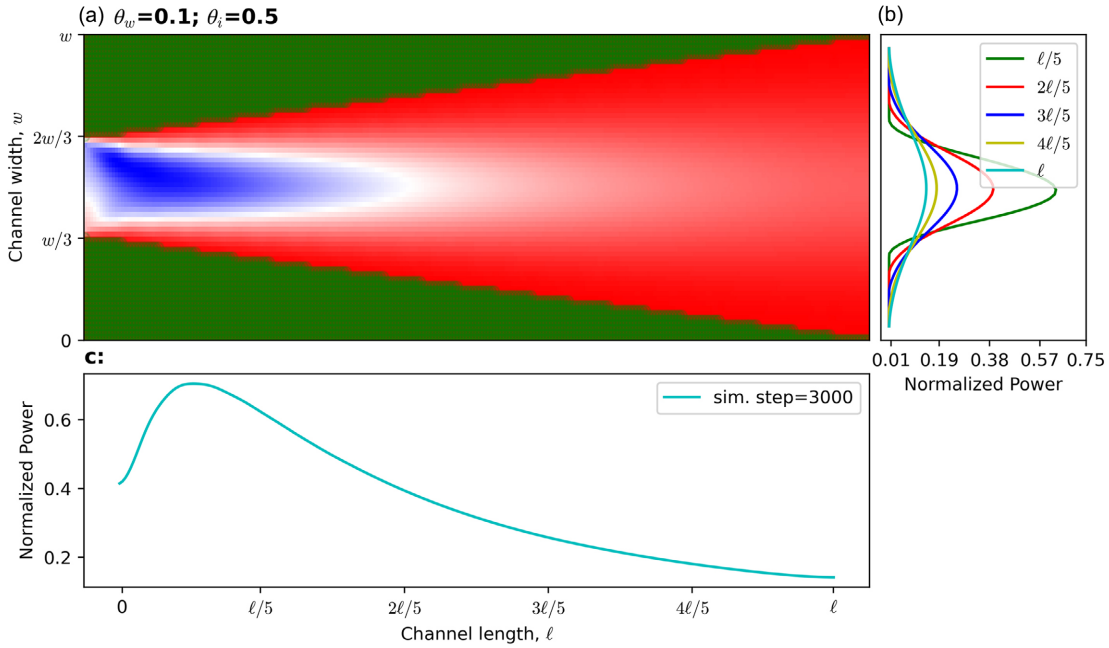

Figure 6. Electric power at inlet temperature, $\theta_i = 0.5$.

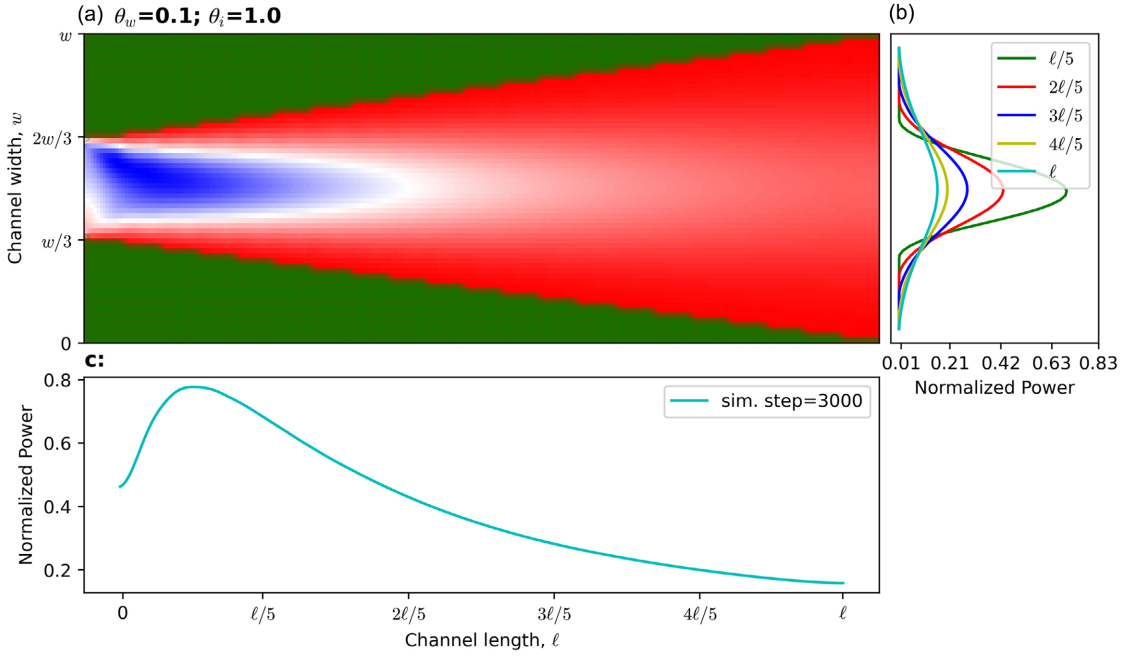

Figure 7. Electric power at inlet temperature, $\theta_i = 1$.

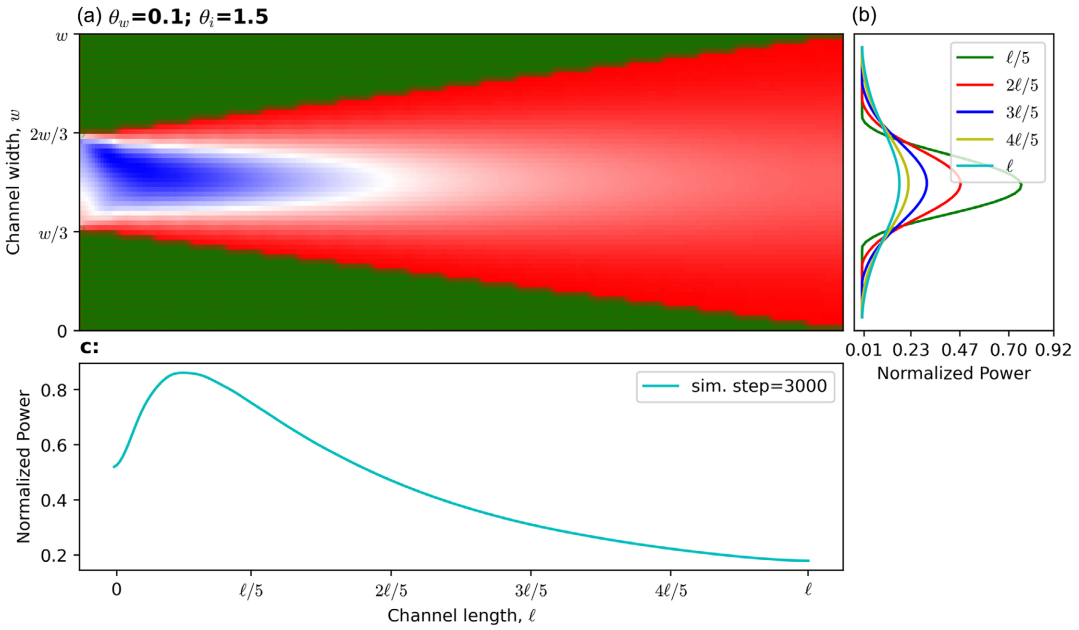

Figure 8. Electric power at inlet temperature, $\theta_i = 0.5$.

However, when the temperature of the working fluid was increased from 0.5 to 1.0 as in **Figure 7**, the electric power rose from 0.5 to peak at 0.8 in the first one-fifth of the channel and declined gradually to stabilize at 0.2 towards the exit, as can be observed in **Figure 7(b)** and **Figure 7(c)**. Therefore, between **Figure 6** and **Figure 7**, the net increase in the peak power produced by a 100% increase in the inlet temperature is 0.1, representing a 14.3% increase in the peak power produced.

Also, in **Figure 8**, an inlet temperature of 1.5 caused the power to increase from 0.5 to peak at 0.9 and declined gradually to stabilize at 0.2 towards the generator's outlet, as in **Figures 8(b)** and **Figure 8(c)**. Therefore, comparing the power produced in **Figure 6** and **Figure 8**, it can be observed that a 200% increase in the inlet temperature of the working fluid, resulted in a 28.6% increase in the peak power.

In all these situations, the increased temperature enhanced the velocity and pressures at the inlet, which facilitates ionization and conductivity of the working fluid, resulting in appreciable electric power in three-fifths of the generator channel. However, towards the exit, a drop in temperature resulted in ion recombination at low temperatures towards the outlet. The low temperature decreased the ionization and conductivity of the working fluid towards the outlet, accounting for the decline in electric power generated in the last two-fifths of the generator channel.

The findings of this study provide insight into the appropriate sections of the MHD generator from which high power can be tapped. The electrical power produced by the heated salt solution (seawater) as working fluid in the MHD power generator would be cheap, renewable, and safe for domestic and industrial use.

5. Conclusions

In this paper, we have mathematically modeled electrical conducting fluid flow in an MHD power generator and conducted a simulation using the Lattice Boltzmann method. The study analyzed the effect of temperature on power generation along different sections of the generator channel. Mathematical modeling helps reduce the cost associated with experimental studies of MHD power generation.

We established that the electric power generated in the MHD generator peaks along one-fifth of the inlet and gradually declines along the generator channel to attain asymptotic stability towards the outlet. The drop in electric power near the outlet region results from ion recombination at reduced temperatures.

Increased temperature increases ionization and enhances the conductivity of the working fluid (salt solution), which enhances electric power generation in the generator.

When the inlet temperature of the working fluid was increased by 100%, the electric power increased by 14.3%, and when it was further increased by 200%, the power increased by 28.6%.

To tap maximum electric power, electrodes should be placed three-fifths along the generator channel where significant power is generated.

Further work in this area would consider the effect of different MHD channel geometries on MHD power generation.

Acknowledgements

The authors appreciate all Reviewers of this manuscript for their valuable contributions.

Conflicts of Interest

The authors have no competing interests to declare that are relevant to the content of this article.

References

[1] Sivasubramanian, S. (2017) Analysis on Performance of Magneto Hydro Dynamics Power Generation. *International Journal of Engineering Research & Technology*, **5**, 5-7.

[2] Krishan, V. (1999) Magnetohydrodynamics of Conducting Fluids. In: Krishan, V., Ed., *Astrophysics and Space Science Library*, Springer, 117-195. https://doi.org/10.1007/978-94-011-4720-0_4

[3] Awais, M., Raja, M.A.Z., Awan, S.E., Shoaib, M. and Ali, H.M. (2021) Heat and Mass Transfer Phenomenon for the Dynamics of Casson Fluid through Porous Medium over Shrinking Wall Subject to Lorentz Force and Heat Source/sink. *Alexandria Engineering Journal*, **60**, 1355-1363. https://doi.org/10.1016/j.aej.2020.10.056

[4] Bera, T.K. (2020) A Magnetohydrodynamic (MHD) Power Generating System: A Technical Review. *IOP Conference Series: Materials Science and Engineering*, **955**, Article 012075. https://doi.org/10.1088/1757-899x/955/1/012075

[5] Li, Y., Li, Y., Lu, H., Zhu, T., Zhang, B., Chen, F., *et al.* (2011) Preliminary Experi-

mental Investigation on MHD Power Generation Using Seeded Supersonic Argon Flow as Working Fluid. *Chinese Journal of Aeronautics*, **24**, 701-708. https://doi.org/10.1016/s1000-9361(11)60082-4

[6] Ajith Krishnan, R. and Jinshah, B.S. (2013) Magneto Hydrodynamic Power Generation. *International Journal of Scientific and Research Publications*, **3**, 1-11.

[7] Sene, F., Caicedo, C. and Fahimi, B. (2022) Spin Hydrodynamic Power Generation and Its Influence on Magnetohydrodynamic Effects. *Open Journal of Fluid Dynamics*, **12**, 213-229. https://doi.org/10.4236/ojfd.2022.122010

[8] Rosa, R.J., Krueger, C.H. and Shioda, S. (1991) Plasmas in MHD Power Generation. *IEEE Transactions on Plasma Science*, **19**, 1180-1190. https://doi.org/10.1109/27.125040

[9] Tanaka, M., Aoki, Y., Zhao, L. and Okuno, Y. (2016) Experiments on High-Temperature Xenon Plasma Magnetohydrodynamic Power Generation. *IEEE Transactions on Plasma Science*, **44**, 1241-1246. https://doi.org/10.1109/tps.2016.2565600

[10] Wang, Y., Cheng, K., Xu, J., Jing, W., Huang, H. and Qin, J. (2024) Novel Onboard High-Power Electricity Generation System of Closed-Brayton-Cycle Enhanced by Multi-Stage LMMHD Generators: Coupling Analysis with Propulsion System. *Applied Thermal Engineering*, **257**, Article 124250.

[11] Ork, K., Masuda, R. and Okuno, Y. (2024) Fundamental Experiment and Numerical Simulation of Ne/Xe Plasma Magnetohydrodynamic Electrical Power Generation. *Journal of Propulsion and Power*, **40**, 368-379. https://doi.org/10.2514/1.b39352

[12] Kimsor, O., Kodera, Y. and Okuno, Y. (2023) Fundamental Experiment and Numerical Simulation of Pre-Ionized Inert Gas Plasma MHD Electrical Power Generation. *Electrical Engineering in Japan*, **216**, e23449. https://doi.org/10.1002/eej.23449

[13] Domínguez-Lozoya, J.C., Domínguez-Lozoya, D.R., Cuevas, S. and Ávalos-Zúñiga, R.A. (2024) MHD Generation for Sustainable Development, from Thermal to Wave Energy Conversion: Review. *Sustainability*, **16**, Article 10041. https://doi.org/10.3390/su162210041

[14] Aoki, M. and Takeda, M. (2022) Study on the Effect of Magnetic Field on Seawater Electrolysis Using a Channel Flow Cell to Simulate a Linear-Type Seawater Magnetohydrodynamic Power Generator. *Chemistry Letters*, **51**, 542-545. https://doi.org/10.1246/cl.220047

[15] Takeda, M., Okuji, Y., Akazawa, T., Liu, X. and Kiyoshi, T. (2005) Fundamental Studies of Helical-Type Seawater MHD Generation System. *IEEE Transactions on Applied Superconductivity*, **15**, 2170-2173. https://doi.org/10.1109/tasc.2005.849604

[16] Foldes, R., Lévêque, E., Marino, R., Pietropaolo, E., De Rosis, A., Telloni, D., *et al.* (2023) Efficient Kinetic Lattice Boltzmann Simulation of Three-Dimensional Hall-Mhd Turbulence. *Journal of Plasma Physics*, **89**. https://doi.org/10.1017/s0022377823000697

[17] Mora, P., Morra, G. and Yuen, D.A. (2019) A Concise Python Implementation of the Lattice Boltzmann Method on HPC for Geo-Fluid Flow. *Geophysical Journal International*, **220**, 682-702. https://doi.org/10.1093/gji/ggz423

[18] Mohamad, A. (2011) Lattice Boltzmann Method, Volume 70. Springer.

[19] Xiong, W. and Zhang, J. (2011) A Two-Dimensional Lattice Boltzmann Model for Uniform Channel Flows. *Computers & Mathematics with Applications*, **61**, 3453-3460. https://doi.org/10.1016/j.camwa.2010.02.040

[20] Jamali Ghahderijani, M., Esmaeili, M., Afrand, M. and Karimipour, A. (2017) Numerical Simulation of MHD Fluid Flow Inside Constricted Channels Using Lattice

Boltzmann Method. *Journal of Applied Fluid Mechanics*, **10**, 1639-1648. https://doi.org/10.29252/jafm.73.245.27885

[21] Miyan, M. (2018) Analysis on the MHD Power Generation Technology. *World Wide Journal of Multidisciplinary Research and Development*, **4**, 309-313.

[22] Krüger, T., Kusumaatmaja, H., Kuzmin, A., Shardt, O., Silva, G., and Viggen, E.M. (2017) The Lattice Boltzmann Method. Springer International Publishing, 4-15.

[23] Wu, L., Tsutahara, M. and Tajiri, S. (2007) Finite Difference Lattice Boltzmann Method for Incompressible Navier-Stokes Equation Using Acceleration Modification. *Journal of Fluid Science and Technology*, **2**, 35-44. https://doi.org/10.1299/jfst.2.35

[24] E-sparX (2020) Magneto-Hydrodynamics (MHD) Generator-Non-Conventional Energy System. YouTube Video.

Nomenclature

α_0	Thermal Diffusion coefficient	f_α	Velocity distribution function
β_T	Thermal expansion coefficient	f^{eq}	Velocity equilibrium distribution function
η	Magnetic diffusivity	h_α	Thermal distribution function
θ_i	Dimensionless inlet Temperature	h^{eq}	Thermal equilibrium distribution function
θ_w	Dimensionless wall Temperature	l	Length of the channel
κ	Thermal conductivity	P	Pressure
ν	Dynamic viscosity	$\overline{P}$	Electrical power
ξ	Non-discretized velocity	S_t	Thermal Source term
ρ	Density of Working Fluid	S_u	Momentum source term
σ	Electrical conductivity	t	Time
τ	Relaxation time	T	Temperature
τ_m	Magnetic relaxation time	T_w	Temperature at wall (Electrode)
τ_T	Thermal relaxation time	u	Velocity in x-direction
Ω	Collision operator	v	Velocity in y-direction
B	Magnetic field	w_α	Lattice weights
B_{ind}	Induce Magnetic field	w	Width of channel
c_α	Discrete velocity	z_α	Magnetic distribution function
c_s	Speed	z^{eq}	Magnetic equilibrium distribution function